Chapter 6
Optical Fiber Sensors

Ming Ding and Gilberto Brambilla

Abstract Fiber optics represents a platform suitable for the monitoring of numerous physical properties. In biology and medicine, optical fibers have found a range of applications ranging from diagnosis to therapy such as cavitational and endoscopic laser surgery. This chapter reviews optical fibers and their wealth of applications in biomedical sensing: from cellular microenvironment to pH, gas, temperature, pressure, and blood flow.

6.1 Optical Fibers

6.1.1 Solid Core Fibers

Optical fibers are cylindrical waveguides that generally consist of an inner glass core with a refractive index n_1, surrounded by a glass or polymeric cladding of lower refractive index n_2—and are often covered by layers of a plastic coating (Fig. 6.1).

Optical fibers are frequently classified as single-mode fibers or multi-mode fibers according to the number of modes supported by the core. If the core refractive index profile is uniform, the fiber is called a "step-index fiber", while if it gradually decreases along the radial coordinate, the fiber is called a "graded-index fiber". In glass optical fibers, the core is typically made from a silicate glass doped with oxides of germanium, phosphorus and other elements in smaller amounts, while the cladding is made of pure silica or fluorosilicate glasses. Index guiding fibers have also been

M. Ding
School of Instrument Science and Opto-electronics Engineering, Beihang University, Beijing 100191, People's Republic of China
e-mail: mingding@buaa.edu.cn

G. Brambilla (✉)
Optoelectronics Research Centre, University of Southampton, Southampton SO17 1BJ, UK
e-mail: gb2@orc.soton.ac.uk

R. De La Rue et al. (eds.), *Biomedical Optical Sensors*,
Biological and Medical Physics, Biomedical Engineering,
https://doi.org/10.1007/978-3-030-48387-6_6

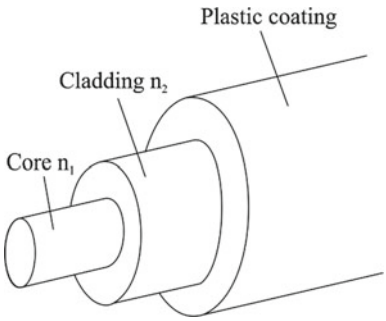

Fig. 6.1 Optical fiber geometry

fabricated from polymers, natural fibers (i.e. silk) and liquid materials, but their applications in the biomedical field have been somewhat restricted.

6.1.2 Microstructured Fibers

Glass and polymer fibers have also been manufactured from a single solid material. These fibers, often called microstructured fibers or photonic crystal fibers (PCFs), are structures where guiding is achieved by a regular spatial distribution of micrometre size air holes [120]. By tailoring the hole sizes and positions, microstructured fibers can vary the dispersion and confinement—and even confine light in a lower refractive index hollow core. Microstructured fibers are often classified into two categories: solid-core and hollow-core fibers.

In the solid-core microstructured fibers (Fig. 6.2a), waveguiding occurs through total internal reflection, in a similar manner to that of traditional optical fibers, with a central core that has a refractive index larger than the average refractive index of the cladding. However, there is no definite boundary between the solid-core region and the air-hole cladding region.

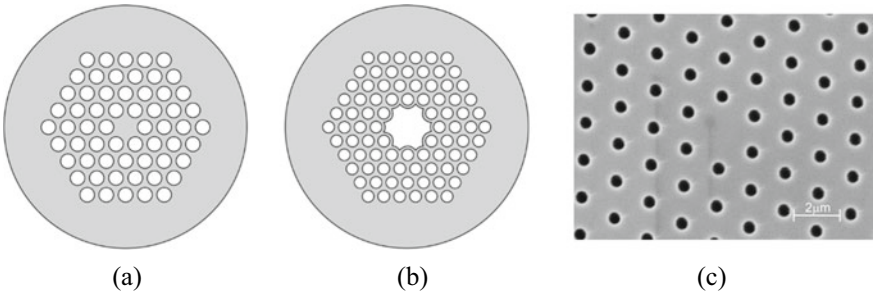

Fig. 6.2 Schematic diagram of **a** a solid-core PCF and **b** a hollow-core photonic crystal fiber (PCF); **c** SEM image of the PCF core region

In hollow-core microstructured fibers (Fig. 6.2b), the air-guided mode has an effective index that is lower than the effective index of the cladding. This type of fiber requires strict control of the periodic cladding structures, since guiding strongly depends on the fiber geometry, with the holes and the related pitch having micrometre dimensions (Fig. 6.2c). Because of the limited applications to biomedical sensing, only fibers having a core refractive index that is larger than the cladding refractive index will be considered in this chapter. These optical fibers are often called index guiding fibers.

6.1.3 Optical Micro/Nanofibers

Optical micro/nanofibers (MNFs) are optical fibers that have been tapered until their uniform waist region has a size comparable to the wavelength. MNFs are fabricated by heating conventional optical fibers to the softening temperature under a moderate degree of stretching [16]. This results in a micrometric optical fiber that is connected by biconical tapers [13, 134] to other fiberized components. MNFs have been manufactured in numerous different optical materials, including bismuthate [17] lead silicate [17], phosphate [146], tellurite [146], and chalcogenide glasses [92]—and a variety of polymers [47, 49, 54, 102, 159]. The extraordinary optical properties exhibited by MNFs include large evanescent fields, strong optical confinement, flexibility, configurability and robustness. Such desirable features have made MNFs an excellent platform for applications in sensing. Light propagation in MNFs is easily explained by refractive index guiding, where the core is effectively the optical fiber material and the cladding is represented by the surrounding medium, usually air or an aqueous solution.

6.1.4 Light Propagation

The propagation of light in index guiding fibers is usually explained either in terms of rays or of waves [106, 129]. In the ray theory, a light ray entering the fiber from a medium with a refractive index n_0 is reflected at the boundary between the fiber core and the fiber cladding (Fig. 6.3). If the incident angle is smaller than θ_{NA}, then the reflection angle at the core/cladding interface is greater than the critical angle θ_{c}, and the light is totally reflected; θ_{NA} is therefore called the maximum acceptance angle. If the medium outside the optical fiber is air with a refractive index value of $n_0 \approx 1$, the application of Snell's law at the air-fiber and at the core-cladding interfaces provides an expression for θ_{NA}:

$$\sin\theta_{\mathrm{NA}} = \sqrt{n_1^2 - n_2^2} = n_1 n\sqrt{2\Delta} = \mathrm{NA} \tag{6.1}$$

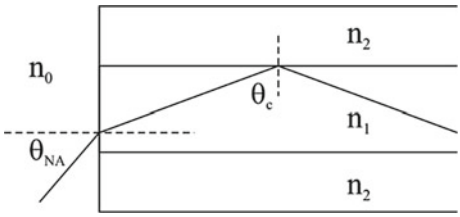

Fig. 6.3 Ray propagation by total internal reflection at the core/cladding interface in optical fibers. $\theta_c, \theta_{NA}, n_1, n_2$, and n_0 represent the critical angle at the core-cladding interface, the incident angle at the optical fiber end surface and the refractive indices of the core, the cladding and the air, respectively

where NA is the numerical aperture of the fiber and $\Delta = (n_1 - n_2)/n_1$ is the normalized refractive index difference.

In wave theory, the solution of Maxwell's equations provides orthonormal field distributions called "modes". Assuming a step index profile, the solution of Maxwell's equations in cylindrical coordinates leads to the propagation equation:

$$\frac{\mathrm{d}^2\psi}{\mathrm{d}r^2} + \frac{1}{r}\frac{\mathrm{d}\psi}{\mathrm{d}r} + \frac{1}{r^2}\frac{\mathrm{d}\psi}{\mathrm{d}\phi} + \left(k^2 - \beta^2\right) = 0 \tag{6.2}$$

where ψ is the wave function of the guided light, r is the radial coordinate, ϕ is the azimuthal coordinate, k is the wave vector in the medium and β is the modal propagation constant.

If the wave-function is assumed to be a propagating wave, then the solutions of (6.2) are expressed by linear combinations of Bessel functions. The boundary conditions require that the optical field has a finite value on the axis ($r = 0$) and tends to zero for very large distances from the fiber axis ($r \to \infty$), providing an easy mathematical formulation for the longitudinal field components:

$$\begin{aligned} &A J_v(ur/a)e^{iv\phi} \quad \text{for } r < a \text{ (in the core)} \\ &B K_v(wr/a)e^{iv\phi} \quad \text{for } r > a \text{ (in the cladding)} \end{aligned} \tag{6.3}$$

where $J_v(ur/a)$ and $K_v(wr/a)$ are Bessel functions of the first and second kind, and $u^2 = \left(k_1^2 - \beta^2\right)a^2$, $k_1 = 2\pi n_1/\lambda_0$, $w^2 = \left(\beta^2 - k_2^2\right)a^2$, $k_1 = 2\pi n_2/\lambda_0$ and $w^2 + u^2 = V^2$.

The functions in (6.3) are called guided modes and are quantised. While J_v represents the fraction of the mode propagating inside the core, K_v describes the fraction of the mode which lies outside the core and is often called the "evanescent field". A specific geometry and refractive index profile can support only selected values of the propagation constant β. The parameter V is related only to the optical fiber geometry:

$$V = \frac{2\pi a}{\lambda_0}(NA)^2 \tag{6.4}$$

and determines the number of modes supported by an optical fiber waveguide: at $V < 2.405$, only a single-mode, designated as HE_{11}, is supported, while at $V > 2.405$ the number of modes increases with increasing V and asymptotically tends to $V^2/2$. It is important to note that the fibers that are commonly called 'single-moded' in reality support two modes with orthogonal polarizations—and the HE_{11} mode is therefore said to be degenerate. Moreover, the choice of angular position is arbitrary, as the mode is a continuously angularly degenerate mode—i.e. it has infinite degeneracy in the azimuthal coordinate.

In most practical fibers, the normalized index difference Δ is on the order of 1% and therefore the approximation $n_2/n_1 \approx 1$ is applicable, which is called the weak-guidance approximation [127, 128]: the modes are called linearly polarized [44] and designated as LP modes. The fundamental mode is designated as LP_{01}.

6.1.5 Optical Fiber Sensor Technologies

Fiber optics represents a platform that can be applied to the sensing of a number of physical properties, including displacement, temperature, pressure, rotation, sound, strain, magnetic field, electric field, radiation, flow, liquid level, chemical analysis, and vibration, to cite just a few examples.

Optical fiber sensors are commonly grouped into *distributed* or *point* sensors, according to whether their sensing can be performed along the length of the fiber or at a specific single position, usually at one extremity of the fiber. They can also be divided according to the output used to evaluate a measurand: phase or intensity [28, 43, 45, 46].

Intensity-based sensors rely on external physical perturbations, or mechanical transducers in close contact with the fiber, to produce a change in the transmitted intensity, usually through increased attenuation, bending, reflection, scattering, or fluorescence. Intensity-modulated sensors can use large core fibers (or fiber bundles) and cheap detection systems—and have therefore found widespread application in industry.

Phase-based sensors evaluate the change in the phase of the signal propagating in a sensing fiber, usually by comparison with a reference in an interferometer. Figure 6.4 shows a schematic diagram of a typical Mach-Zehnder interferometer: light from a laser source is split into a reference fiber unaffected by external perturbations and a sensing fiber that is exposed to the surrounding environment—and the light is then recombined by means of a fiber coupler, before reaching a detector. If the two components are exactly in phase upon recombination, they interfere constructively—while, if they are out of phase, destructive interference occurs. The two components are usually deliberately placed in quadrature, meaning that a small change in the environmental conditions results in the maximum relative change in intensity.

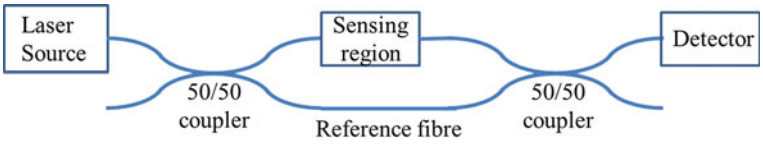

Fig. 6.4 Schematic of a sensor based on the Mach-Zehnder interferometer. Light is injected from a laser source into a 50/50 coupler, where it is split in two equal parts traveling through a reference fiber and a sensing fiber, respectively. In the sensing fiber the signal experiences a phase delay which, when recombined with the reference at the second 50/50 coupler, is measured by the detector in the form of an intensity change due to interference

In general, phase-based sensors have a higher accuracy and a much larger dynamic range than intensity-based sensors, since phase-differences can be measured with extreme precision, often to down to the tens of μrad level, within a very broad range. Yet, phase-modulated sensors often require a more expensive detection system—and therefore have application in the distributed sensing market, where the cost per unit of length is small.

Amongst the point sensors, a significant fraction of the industrial implementations has relied on fiber gratings, which are structures inscribed in the fiber core by periodically changing the refractive index. There are two types of gratings: Fiber Bragg Gratings (FBGs) and Long Period Gratings (LPGs). While the former has a period comparable to the wavelength of the light propagating in the core—and couples forward propagating core modes with backward propagating core modes, the latter is characterised by a period that is orders of magnitude larger than the wavelength and couples forward propagating core modes with cladding modes [37]. Because of the relatively strong photosensitivity effects exhibited by optical fibers when exposed to ultraviolet light, fiber grating fabrication has widely exploited ultraviolet lasers, often in conjunction with phase masks (for FBGs) or amplitude masks (for LPGs).

6.2 Sensors

Biological and medical sensing have benefited extensively from the use of optical fibers, because of their minimal cross section, negligible loss and extreme flexibility. Indeed, it is widely recognised that optical fibers found applications in medical imaging well before their application in telecommunications: in 1954 fiber bundles were successfully deployed in endoscopy [62]—providing easy access to otherwise inaccessible parts of the human body and thereby paving the way to beam delivery for endoscopic laser surgery.

This section will review the wealth of applications of optical fibers in biosensors that have arisen since their first deployment in endoscopy. This review will include biomolecule sensing, blood flow, gas, pressure, pH, and temperature.

6.2.1 Biomolecules

Optical fiber biosensors mostly use surface functionalization with biological molecules, such as antibodies or enzymes, that show high selectivity for a specific analyte. When the analyte binds to the functionalised surfaces, there is a change in an optical property (typically absorption, refractive index, luminescence, fluorescence emission or quenching) that can then be used for detection. Biomolecular sensing can be carried out in two distinct configurations, i.e. by exploiting the mode evanescent field along the direction of propagation—or in the so-called optrode configuration.

In the optrode configuration, the distant fiber end is functionalised with recognition biomolecules (Fig. 6.5) and the optical fiber simply delivers light to the sensing region at the fiber tip—and then collects it, after reflection, back to the detector. Functionalizing molecules are frequently encapsulated inside a polymer, a membrane or beads [11, 15, 41, 57, 85, 147] that often also perform the additional task of concentrating the analyte to be detected. Although the sensor selectivity in optrode biosensors can be extremely high, the sensitivity is limited by the size of the functionalised area and by the concentration of recognition molecules at the surface.

When the signal to be detected is considerably smaller than that used for excitation, collection can be performed using a second fiber, a CCD (charge coupled device) camera or an inverted fluorescence microscope. This method found large application in the simultaneous detection of multiple analytes using fiber bundles [2, 39, 57], where each single core transmits information about a single analyte. Microstructured fibers have been widely deployed in sensors exploiting fluorescence because the air holes provide easily functionalisable surfaces in close proximity to the core evanescent field. α-streptavidin and α-CRP (cancer-reactive protein) antibodies have been functionalised inside polymer microstructured fibers and fluorescence—and have provided a detection limit of 80 nM when analysing a sample volume of 27 μL [64].

A sensor configuration exploiting evanescent fields was first proposed in 1965 [60]—and later applied to immunoassays [80]. In this class of sensors, the evanescent field overlaps with recognition molecules bound to the fiber surface (Fig. 6.6). As the mode propagating in the core has an extremely small overlap with the cladding surface, part of the cladding is usually removed from the fiber until the guided mode has a significant overlap with the molecules in the solution. The evanescent

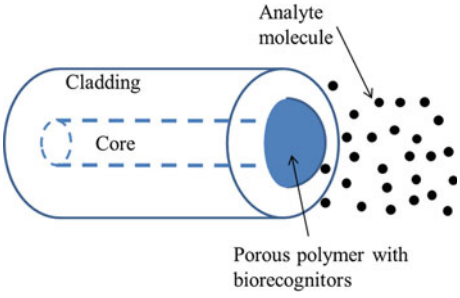

Fig. 6.5 The optrode configuration: a biological recognitor is immobilized at the distant end of an optical fiber, where it interacts with the analyte molecules in solution

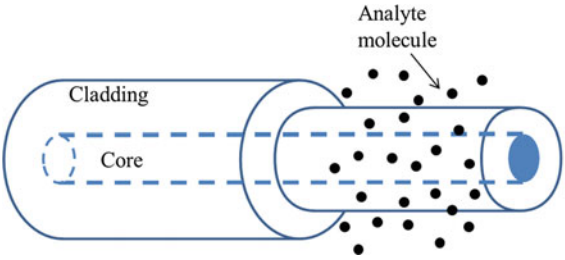

Fig. 6.6 Evanescent wave biosensors: part of the cladding is etched away and interaction between the mode propagating in the core and the analyte occurs at the side surface of the fiber where recognition molecules can be immobilized

field is extremely sensitive to the refractive index at the sensor surface—and any change that modifies the refractive index of the surface, such as binding of analyte to an immobilized recognition molecule, will result in the change of the propagation properties of the mode. The evanescent field generated within the medium or cladding decays exponentially with the distance from the core surface and its penetration depth, defined as the distance at which the field strength decays to $1/e$ of its value at the interface, is comparable to the wavelength of light. The detectable optical changes are therefore limited to a small region in close proximity to the fiber surface, with relatively little interference from the bulk solution.

Because of the large surface area available in their voids, microstructured fibers have found a prompt application in biomolecular sensing. Selective detection of α-streptavidin and Cy5-labelled α-CRP antibodies in series, at preselected positions, was demonstrated using a single piece of microstructured fiber fabricated from a cyclic olefin copolymer and serial fluorescence-based selective sensing [36]. The sensitivity and detection limit of sensors based on microstructured fibers are strongly dependent on the overlap between the mode and the analyte—and the fiber cross section geometry can be optimised for aqueous or gas detection [56]. Long period gratings have been used to improve the overlap in refractometers, providing a maximum sensitivity of 1500 nm/RIU at a refractive index of 1.33, and a detectable index change of $2 \cdot 10^{-5}$, two orders of magnitude larger than the sensitivity observed for a long-period grating in a standard optical fiber [117]. Long period gratings in microstructured fibers have also been used to determine the thicknesses of a monolayer of poly-L-lysine and double-stranded DNA, with a sensitivity of 1.4 nm/1 nm in terms of the shift in resonance wavelength in nanometre per nanometre thickness (l nm) of the biomolecular layer [116].

MNFs have a very strong evanescent field and have therefore been used to detect biomolecules in close vicinity to the waist region (Fig. 6.7). Stiebeiner et al. [135] performed spectroscopy of 3,4,9,10-perylenetetracarboxylic dianhydride molecules (PTCDA) using between 1 and 10 mm long MNFs that had as little as 100 nm diameter. Optimized surface spectroscopy of organic molecules was performed by Warken et al. [153], who measured sub-monolayers of 3,4,9,10-perylene-tetracarboxylic dianhydride (PTCDA) molecules with a 500 nm diameter, 3 mm long, MNF—and showed that the sensitivity exceeds free-beam absorption spectroscopy by several orders of magnitude. Takiguchi et al. [140] used MNFs with a diameter of 410 nm

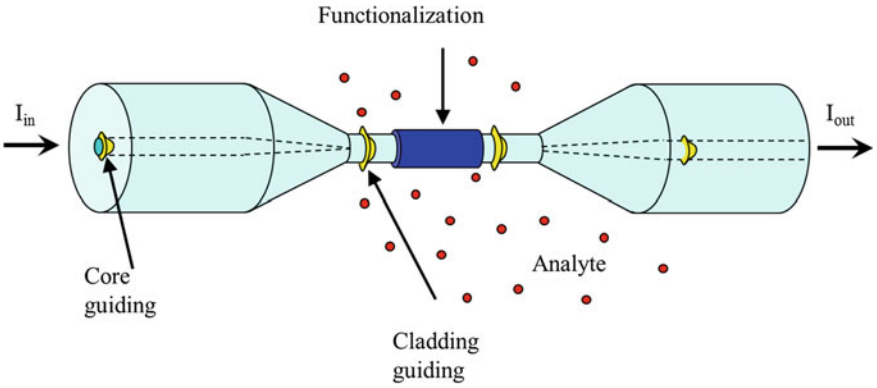

Fig. 6.7 Schematic diagram of a coated MNF for bio-chemical sensing

for saturated absorption spectroscopy of the acetylene (C_2H_2) $\nu 1 + \nu 3$ band transitions. Vishnoi et al. [149] demonstrated a spectrophotometer based on a tapered multimode fiber and used it to measure dye solutions with concentrations as low as 1 ppm in water. A 900 nm diameter MNF embedded in a 125 mm wide micro-channel with a detection length of 2.5 cm was used by Zhang et al. [163] to measure the absorbance of methylene blue (MB)—with a detection limit of 50 pM within the operational range of 0 to5 nM. The sensor was also functionalised to test bovine serum albumin (BSA) and achieved a detection limit of 10 fg.mL^{-1}.

A 3.69 μm-diameter, 7.1 mm-long MNF was used by Wiejata et al. [157] to detect a fluorescein solution at concentrations of 10–60 μM by exciting it at a wavelength of 460 nm and collecting the fluorescence emitted at 516 nm. Tian et al. [144] used a micro-channel chip designed for the label-free bio-testing of an IgG antibody-antigen pair to detect biomolecules, exploiting the modal interference that occurs along a non-adiabatic MNF. Wang et al. [152] modelled a bio-sensor using the effective phase shift in a fiber Bragg grating inscribed in a MNF. Proteins and DNA adsorbed on the surface were detected with a detection limit of 3.3 pg.mm^{-2}—by using the stop-band degeneracy and its application to refractive index sensing.

6.2.2 Single Cell Environments

Cellular micro-environments at the single cell level have been monitored by using MNF tips [141], since these allowed for a respective reduction in probe size, sample volume and response time of three, six and two orders of magnitudes with respect to the equivalent conventional optical sensor based on conventional 125 μm diameter optical fibers. In its easiest configuration, the sensor head is excited by light launched into its fiber pigtail and the resulting evanescent field at the MNF tip is used to excite target molecules bound to the antibody molecules (Fig. 6.8); the fluorescence

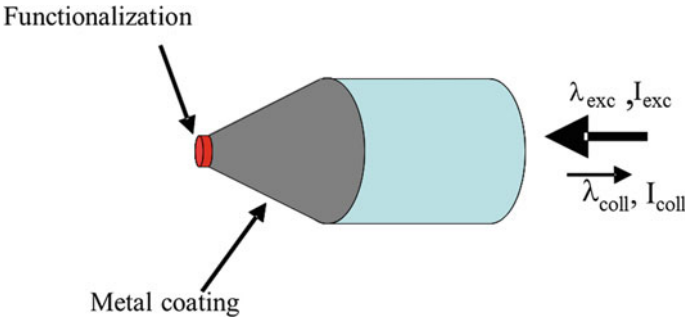

Fig. 6.8 Schematic diagram of a functionalized MNF tip for selective bio-chemical sensing

emission from the analyte molecules is then collected and analysed in the same fiber pigtail. MNF tips of 30–50 nm diameter [150] were covalently bound with antibodies that selectively target analyte molecules within the cellular microenvironment: this included benzo[α]pyrene [71], benzo[α]pyrene tetrol (BPT) [27] and caspase-9 [70]. A detection limit of ~0.64×10^{-11} M was reported for BPT.

DNA/RNA detection without the need for a dye-labelled target molecule or an intercalation reagent in the testing solution was demonstrated using fluorescence-based MNF biosensors [88]. Experimental results showed that the concentration and the mass detection limits for a sub-micron diameter MNF tip are 10 nM and 0.27 aM, respectively. MNF tips have also been used to detect telomerase in the nucleus of living MCF-7 cancer cells [165]. The encapsulation of dextran-linked fluorescence indicators in an organic hydrogel [111] enabled the co-immobilization of different indicators.

An intensity-based sensor in a compact micro-ball lens structure fabricated at the cleaved tip of a MNF coupler was proposed [55] for sensing the glucose concentration in deionized water. A sensitivity of 0.26 dB/% was achieved for a concentration change from 0 to 12 volume %, with the output intensity of the sensor decreasing linearly from −57.4 to −60.5 dBm.

6.2.3 Potential of Hydrogen (pH) Measurement

pH is often considered to be the single most important indicator in medicine, as it is strictly related to the correct operation of many organs of the human body. pH is frequently measured by a chromophore or by absorption-based indicators. In the first configurations demonstrated, optical fiber pH sensors used phenol red, covalently bound to polyacrylamide microspheres, as an indicator. The microspheres were inserted in a cellulose dialysis tube connected to two large-core plastic fibers, which were in turn inserted into a blood vessel through a needle. In vivo testing was carried out by detecting extracellular acidosis during regional ischemia in dog

hearts [138], conjunctival pH [1], and pH gradients in canine myocardial ischemia [155]. The first fiberized sensor for the simultaneous monitoring of pH, oxygen and carbon dioxide concentrations relied on three optical fibers enclosed in a polymer tube [42]. The pH measurement was carried out using hydroxypyrene trisulphonic acid attached to a cellulose matrix at the fiber tip.

The measurement of pH level in the stomach and oesophagus is extremely important for monitoring of the human foregut. One of the first sensors demonstrated used two fluorophores, fluorescein and eosin, immobilized in amino-ethyl cellulose particles fixed on polyester foil [7, 103]. Another sensor used two absorbance dyes, meta-cresol purple and bromophenol blue, attached to polyacrylamide microspheres. Although the accuracy achieved, better than 0.1 pH units, satisfied clinical requirements, the response time, between 1 and 6 min depending on the pH step, was considered too long—so long that it would prevent detection of any rapid change of pH, like the detection of gastro-oesophageal reflux, where pH changes occur over time scales shorter than 1 min). A third sensor [8] used two chromophores, bromophenol blue (BPB) and thymol blue (TB), fixed at the end of plastic optical fibers, to form a very thin pH-sensitive layer with an accuracy of the order of 0.05 pH units. A pH sensor using an acid-base indicator covalently immobilized on the core of a 200/380 μm fiber demonstrated a detection limit of 0.05 pH units [9].

A multi-layered assembly of poly(allylamine hydrochloride) and poly(acrylic acid) on a 30 μm diameter, 10 mm length MNF was exploited as a pH sensor by detecting the wavelength shift associated with changes in the pH level [130]—and provided a sensitivity of 87.5 nm/pH unit between pH 4 and 6, a response time of 60 s and a detection limit of 0.05 pH units.

6.2.4 Oxygen and Carbon Dioxide

The continuous monitoring of oxygen (O_2) and carbon dioxide (CO_2) is very important in many biomedical fields, such as cardiovascular and cardiopulmonary systems, and they are therefore the two chemical parameters that have been most investigated for in vivo applications.

Carbon dioxide (CO_2) sensors rely on measurement of the pH of carbonate solutions, as these depend on the amount of CO_2 dissolved in them. All optrodes developed for measurement of blood CO_2 concentration exploit the same dye as utilized for pH measurement, fixed at the fiber end and covered by a membrane permeable to CO_2. In situ measurements use fluorophores, such as hydroxypyrene trisulphonic acid, dissolved in a bicarbonate buffer solution enclosed by a membrane permeable to CO_2. Many optical fiber CO_2 sensors have been described for the detection of CO_2 in blood or in human breath [42, 59, 97]. An optical fiber sensor for the continuous detection of gastric CO_2 has a measurement range of 0–14 kPa, with a resolution of less than 0.1 kPa and an accuracy of 0.27 kPa.

The measurement of oxygen concentration is often performed either spectroscopically, by targeting haemoglobin, or by using a fluorophore the efficiency of which

is strongly affected by the presence of oxygen. The maximum oxygen concentration in blood was the first quantity to be measured optically—by exploiting the different absorption spectra of the haemoglobin and the oxyhaemoglobin in the near infrared [69]. Optical fiber sensors that are capable of being inserted in arteries and veins rely on the collection of reflected or absorbed light in the greatest absorption regions of haemoglobin and oxyhaemoglobin—and the oxygen saturation is calculated as the ratio of the absorptions at the two different wavelengths. The use of multiple wavelengths or of the whole spectrum was proposed [91, 96] to discriminate other haemoglobin derivates. Non-invasive sensors use the light transmitted through body extremities, such as earlobes, toes, or fingertips, but suffer from strong signals from adjacent tissues [122]. Blood oxygen saturation has also been measured in teeth [94] by measuring reflectance in the visible to near-infrared spectral range (typically at 660 and 850 nm). The use of spectrophotometer analysers [40] enabled the real-time measurement of intracapillary haemoglobin oxygenation and concentration, local oxygen uptake rate, local capillary blood flow, changes in subcellular particle sizes, and capillary wall permeability. The tissue was illuminated by a Xenon arc lamp via a bifurcated fiber bundle—and the back-scattered light provided in situ, real-time spectra of small volumes of tissue.

Haemoglobin is fully saturated at ≈100 Torr—and its use for the indirect measurement of oxygen concentration has limited application in the case of the respiration of gas mixtures with oxygen contents larger than 20%, as routinely used in anaesthesia. The first oxygen sensor involving optrodes used perylene-dibutyrate as a fluorophore fixed on amberlite resin beads at the end of two plastic optical fibers that were coated by a hydrophobic membrane permeable to oxygen [109, 133]. In vivo testing was carried out in dog eyes by measuring the fluorophore quenching due to arterial oxygen. A non-invasive sensor measured the oxygen flow at the skin surface to provide information on the oxygen flow inside the underlying tissue [61]: two optrodes based on a ruthenium complex were placed in contact with the skin—and used to measure, in real time, the difference in oxygen pressure across a membrane. An oxygen sensor using MNFs relied on the fluorescence quenching of tris-(1,10-phenanthroline)ruthenium(II) chloride in the presence of oxygen or dissolved oxygen [119] and provided a detection limit of 1×10^{-17} mol with response times shorter than 1 s, in volumes as small as 100 fL.

6.2.5 Temperature

Because of the immunity of fibers to electromagnetic interference, optical fiber thermometry has found application in the controlled heating of biological tissues—e.g. hyperthermia for cancer treatment, the thermal mapping during photoradiation therapy of malignant tumors and the thermodilution technique for blood flow measurement. A number of mechanisms have been proposed, including all-fiber devices [18], the use of transducers [33] or wavelength modulators [75, 108]. In one of its early demonstrations, a reflective fiber Fabry–Perot resonator [75] that

was formed by coating the fiber end-face with a dielectric was used for continuous temperature monitoring in hyperthermia systems, covering the temperature range 25–45 °C, with a resolution better than 0.1 °C. Subsequently, a thermographic phosphor containing rare-earth atoms was bonded to the end of an optical fiber (~ 400 μm core diameter)—and the variation of its fluorescence with the temperature was utilized as a transduction sensing mechanism [156] in the −50 to 200 °C operational range, with an accuracy of 0.1 °C. Long period gratings [66] and fiber Bragg gratings (FBG) have also been exploited for thermometry with a sensitivity up to 175 pm/°C [115]. FBG thermometry has been used to perform distributed measurements in soft-tissue [121] by means of an array of ten gratings. The biocompability of the optical fiber sensor has been a major issue, with a number of coatings such as polyimide, polydimethylsiloxane (PDMS), ethylene-tetrafluoroethylene (or Tefzel®), and poly-tetrafluoroethylene (or Teflon) being investigated for biomedical applications [14, 118]

MNFs have also been used in temperature sensing, in the form of a simple modal interferometer [166], by coating the waist region with a material having a high thermo-optic coefficient. In this design, the interference pattern strongly depends on the refractive index, which in turn depends on the ambient temperature—with an operational range from −20 to 80 °C. The lyotropic liquid crystal decylammonium chloride/water/NH4CI (DACI-LLC) was combined with an MNF to produce a thermometer with an operating range from 40 to 80 °C [148]. Coating the MNF with a sol-gel thin-film that entrapped quantum dots provided variations in photoluminescence with temperature in the range from 30 to 70 °C, with a sensitivity of 1%/°C [162, 163]. An in-line Mach-Zehnder using two cascaded MNFs to excite and recombine the cladding mode with the core mode provided a sensitivity of 0.08 nm/°C over the temperature range from 20 to 60 °C [86, 90]. A 100 μm long intrinsic Fabry–Perot etalon fabricated using a femtosecond laser on the waist of a 30 μm diameter MNF [164] provided the means to measure temperature in the range from 0 to 100 °C, with a sensitivity of 12 pm/°C. Temperature and strain discrimination were achieved by exploiting multimode interference in a tapered core-less multimode fiber [3]: the temperature and strain resolutions were 1.6°C and 5.6 με, respectively. A tapered bend-resistant fiber, with different phase shifts between the inner and the outer cladding modes, provided a temperature sensitivity of −0.0253 rad/°C [89].

The combination of MNFs with Bragg gratings as end-reflectors showed a sensitivity of 9.7 pm/°C between 20 and 70 °C [65]. An MNF coupler tip thermometer was also demonstrated at temperatures up to 1283 °C—with a 2-dimensional resolution of <200 μm, a sensitivity of 11.96 pm/°C—and a detection limit of 0.836 °C for a wavelength resolution of 10 pm [31]. A 4.4 μm long micro-cavity fabricated within an MNF tip section smaller than 10 μm in diameter provided a reflective Fabry–Perot modal interferometer with a temperature sensitivity of 20 pm/°C between 19 and 520 °C, and a detection limit of 0.58 °C [77]. A similar temperature probe using a first-order, 36.6 μm long, FBG fabricated by focused ion-beam machining in a 6.5 μm diameter MNF demonstrated a similar sensitivity of 20 pm/°C and was operated at temperatures up to 500 °C [78]. A shorter device combining an MNF tip and a FBG exhibited a similar temperature sensitivity [38].

Tapered photonic crystal fiber coated with a layer of liquid crystal provided a sensitivity of 0.2 nm/°C within an operational range of 50–78 °C [114, 125]. Microfiber coil resonators embedded in Teflon with opposite thermo-optic coefficients were proposed and demonstrated as a temperature-insensitive device [20, 21] and showed a sensitivity of <6 pm/°C at room temperature.

6.2.6 Pressure

Although pressure sensors have found many applications in medicine [113, 118], most optical fiber pressure sensors have been designed for inclusion in catheters. The early sensors relied on monitoring the movement of mirrors mechanically coupled to pressure-sensitive membranes, which results in the modulation of light reflected and coupled into the output [82, 87, 95]. Applications included intra-muscular [26, 101], intra-cranial [107], cardiovascular [126] and skeletal muscle [124] pressure monitoring, airway pressure monitoring in young [131, 132] and in mechanically ventilated patients [29]—and even urological neurology and urodynamics. A typical fiber optic pressure sensor device is based on a pressure-balancing system: a pressure-sensitive membrane, located in a side hole of the catheter tip, is attached to a cantilever mirror. Under pressure, the membrane deflects the cantilever mirror with respect to the end of the fiber bundle and proportionally alters the intensity of the back-reflected light. Membranes have been positioned either at the distal end of the optical fiber [76, 100] or on the side [110, 142], in order to decrease the artefacts related to biological flow. Another typical fiber optic pressure sensor is based on a bifurcated fiber optic bundle with a pressure-sensitive membrane diaphragm at the end [51]. Although the sensor operated up to a pressure of 3000 mm of mercury (mmHg), the device response was highly nonlinear above 1000 mmHg. Physiological measurements could be performed in the range from 100 to 300 mmHg, with a typical linearity of 0.5% and a temperature shift of 0.1%/°C [50]. This micro-transducer was deployed in the measurement of pressure profiles in urethral conducts [58] and of intra-uterine pressure during labour [136, 137]—and provided results in agreement with those obtained using a catheter-tip bridge strain-gauge transducer [143]. The use of an external Fabry–Perot cavity bonded to the end of the fiber [25, 139] has made it possible to improve the pressure sensitivity, at the expense of the size. Diaphragms made of polymers [22, 23] or silica [34] have been added at the ends of optical fibers that were previously etched to form Fabry–Perot cavities, providing a more robust solution—with a dynamic range of 0–1200 kPa and resolutions of 10 Pa and 30 Pa, respectively.

Other optical fiber pressure transducers have relied on mirror bending rather than displacement [81]: in this design, the light is brought to the diaphragm surface by a cylindrical array of fibers and the reflected light from the diaphragm is then distributed over an array of collection fibers arranged concentrically around the illumination fibers. The pressure is calculated from the ratio of the amount of light received by an outer ring of collection fibers to that from an inner ring with more collection fibers.

More recent manometers have exploited Bragg gratings [5], which enables multiplexing [10] up to a series of seventy-two sensing elements—with a distance of 1 cm separating the adjacent sensing elements. Optical fiber manometry in catheters has shown extremely high sensitivity, enabling immediate applications in colonic diagnostics [4, 6, 32] and high-resolution mapping of the upper gastrointestinal tract [151].

Multiplexing has also enabled easy embedding of sensor fibers in pressure mats [112] with applications in pedobarography [52], which was previously carried out using critical reflection at the interface between plastic and glass [12]. Long period gratings in polymeric fibers [19] have been proposed for pressures up to 150 mbar and showed a sensitivity of 10.5 pm/mbar. Hollow-core microstructured fibers have been used for pressure sensing by selectively blocking cladding air holes by glue sealing and femtosecond laser machining [63]. By immersing the fiber end into a liquid, a compressible Fabry–Pérot cavity was formed in the fiber core of the PCF. A pressure sensitivity of 18.15 nm/kPa was demonstrated experimentally in the pressure range from 110 to 130 kPa.

6.2.7 Blood Flow

The velocity of blood flow in vessels is an important measurable quantity for medical applications, such as thrombosis and strokes, and it has been monitored using laser Doppler flowmetry [67, 79, 98], which relates the Doppler frequency shift of laser light scattered by moving blood to its flow velocity. The fiberized version of laser Doppler flowmetry allows for invasive measurements of blood flow [68]. Figure 6.9 shows the basic scheme for fiber-optic laser Doppler flowmetry: light from a laser is guided by an optical fibre onto the tissue or vascular network being studied, where it is scattered and partially absorbed by the tissue [72]. Light scattered by moving blood cells suffers a Doppler shift, which is analysed by the detector and is then processed to derive the blood flow rate through spectral analysis [99].

This technique has been widely applied in cardiology and has even been used to evaluate phasic blood flow in deeper intramyocardial layers [99]—having been

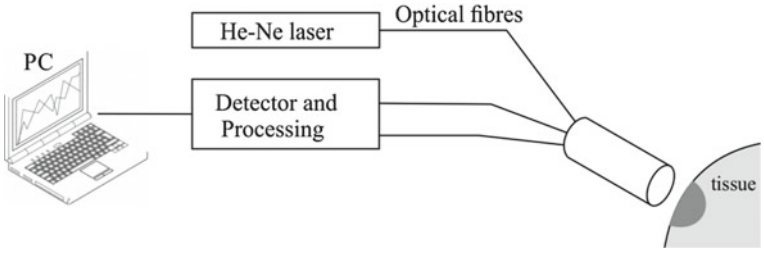

Fig. 6.9 Basic schematic of fiber-optic laser Doppler flowmetry

previously restricted to the epimyocardium because of methodological limitations. It has also been used to visualize and measure non-invasively the middle cardiac vein flow [53]. The use of feedback optical stabilization has been shown to improve significantly the Doppler signal in self-mixing intra-arterial measurements [30]. On the other hand, the target scattering properties have proved to be a major issue that hinders the sensor detection limit [160]. Self-mixing laser Doppler performed on extra-corporeal blood flow has shown that the Doppler shift is generated by erythrocyte cells [104, 105].

6.2.8 Endoscopy

Although many different types of sensor have been developed for applications in the biomedical realm, it is fair to state that the most successful application of optical fibers in healthcare is represented by the endoscope, which has been integrated with gas/liquid delivery lines and cutting tools for keyhole surgery and investigation of symptoms, mostly of the gastro-intestinal and respiratory tracts.

Even though in its original conception the endoscope was designed in the form of an array of small diameter optical fibers that transferred, in a coherent manner, a visual image over a distance of the order of 1 m [35], the most recent research has aimed to replace the use of numerous optical fiber cores (each representing a single pixel) with a single optical fiber supporting thousands of micrometric cores supported by thin struts [158] or with a single solid fiber supporting multiple modes [24, 48]. Multicore fibers made from suspended cores with air claddings have an extremely large numerical aperture—and each core can guide modes at visible wavelengths in a very small, sub-micron diameter—thus reducing the overall size of a single pixel. The use of polarization maintaining cores [73], semi-random arrangements [74] and proximal detection [154] in these multicore fibers allowed also for adaptive multiphoton endomicroscopy, which it has been suggested could allow for internal cell-scale examination, even during neurosurgery.

The use of one multimode fiber (MMF) allows the reduction of the endoscope cross-section by a factor of 20x, thus increasing the endoscope flexibility, while preserving a high resolution [93]. MMF endoscopy has quite suddenly become available because of the development of a device, named the photonic lantern [83, 84], that is capable of relating each mode of an array of optical fibers, to a single mode (or finite linear combination of modes) in an MMF. The photonic lantern has made it possible to transfer the information associated with each single spatial position to a different mode that can propagate in the same physical position as for other modes, thereby reducing the overall footprint of the average endoscope. Additional analysis on the phase relationship between the different modes has been used to focus light transmitted through an MMF to an unprecedentedly small size, to remove lenses at the endoscope ends and to reconstruct images behind the fibers using holographic techniques [24] (Fig. 6.10).

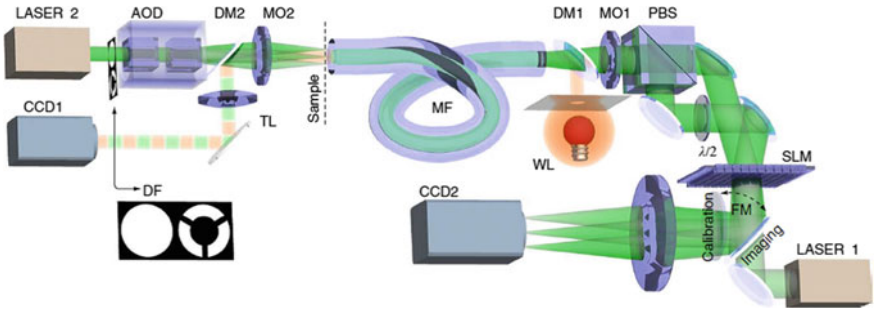

Fig. 6.10 Schematic of the microscopy based on multimode fibres (reproduced with permission from Cižmár and Dholakia [24])

Endoscopy has seen significant development in extending its operational range towards longer wavelengths [123], allowing for thermal imaging of internal organs and easier detection of tumours. Although the intrinsic fragility of chalcogenide glasses and their relatively poor compatibility with biological matter seems to be a major hurdle for the deployment of mid-IR endoscopes in the operating theatre, suitable packaging would solve these issues and allow for additional information on thermal imaging to be made readily available during surgery.

In order to visualize remotely and noninvasively the tissue microstructure and operation with micrometre resolution, optical coherence tomography (OCT) has been integrated within endoscopy, providing real time 3D imaging. Figure 6.11 shows a configuration where an external Michelson interferometer has been used to compensate the optical path difference between the reference and the signal coming from the sample in the endoscopic Fizeau sensing interferometer, which included a graded index lens at its end.

A more significant development in endoscopy could possibly come from the deployment of high power lasers in surgery procedures. In addition to the optical fiber bundles utilised to deliver imaging, current endoscopes include light delivery systems to illuminate the organs—and a channel to deliver medical instruments to manipulate and cut tissues. High power lasers have been used for a variety of material processing tasks and it is not inconceivable to think that in future they will replace the medical instrumentation used within endoscopes to cut and incise biological tissue. Indeed, carbon dioxide (CO_2) and Neodynium YAG lasers have both been advocated for reduction of bleeding during surgery and post-operative ecchymosis [145].

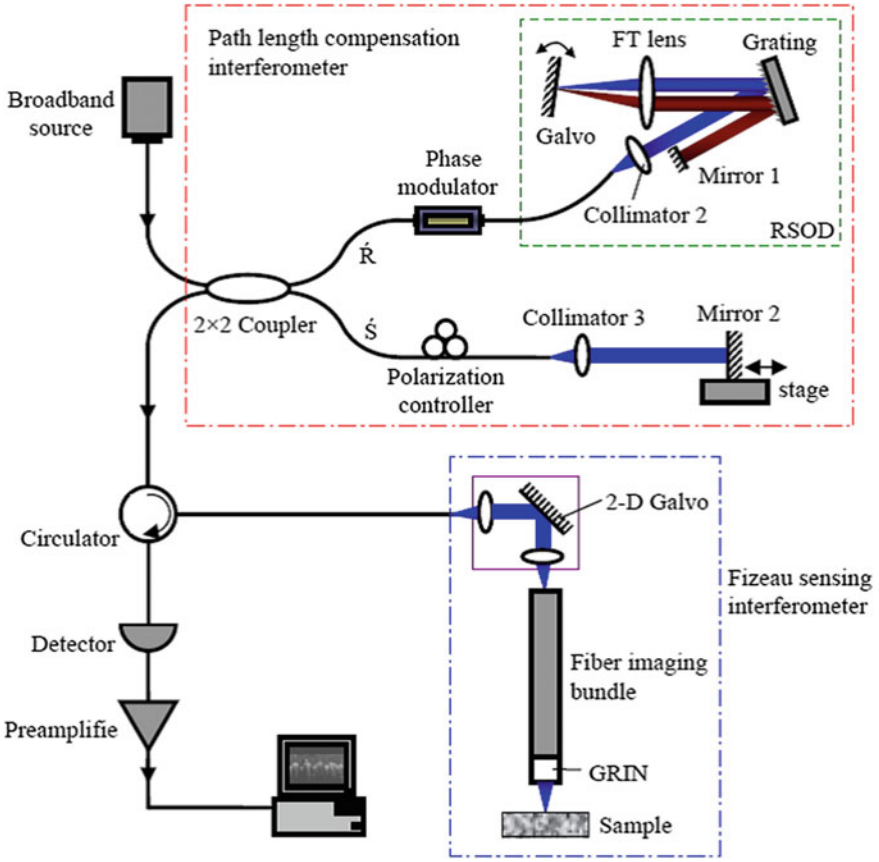

Fig. 6.11 Schematic of an endoscopic OCT with outside path compensator (reproduced with permission from Yang et al. [161])

References

1. E. Abraham, S.E. Fink, D.R. Markle, G. Pinholster, M. Tsang, Continuous monitoring of tissue pH with a fiberoptic conjunctival sensor. Ann. Emerg. Med. **14**, 840–844 (1985)
2. F.P. Anderson, W.G. Miller, Fiber optic immunochemical sensor for continuous, reversible measurement of phenytoin. Clin. Chem. **34**, 1417–1421 (1988)
3. R.M. André, C.R. Biazoli, S.O. Silva, M.B. Marques, C.M.B. Cordeiro, O. Frazão, Strain-temperature discrimination using multimode interference in tapered fiber. IEEE Photonics Technol. Lett. **25**, 155–158 (2013)
4. J.W. Arkwright, I.D. Underhill, S.A. Maunder, N. Blenman, M.M. Szczesniak, L. Wiklendt, I.J. Cook, D.Z. Lubowski, P.G. Dinning, Design of a high-sensor count fibre optic manometry catheter for in-vivo colonic diagnostics. Opt. Express **17**, 22423–22431 (2009)
5. J.W. Arkwright, N.G. Blenman, I.D. Underhill, S.A. Maunder, M.M. Szczesniak, P.G. Dinning, I.J. Cook, In-vivo demonstration of a high resolution optical fiber manometry catheter for diagnosis of gastrointestinal motility disorders. Opt. Express **17**, 4500–4508 (2009)

6. J.W. Arkwright, N.G. Blenman, I.D. Underhill, S.A. Maunder, N.J. Spencer, M. Costa, S.J. Brookes, M.M. Szczesniak, P.G. Dinning, A fibre optic catheter for simultaneous measurement of longitudinal and circumferential muscular activity in the gastrointestinal tract. J. Biophotonics **4**(4), 244–251 (2011)
7. F. Baldini, P. Bechi, S. Bracci, F. Cosi, F. Pucciani, In vivo optical-fibre pH sensor for gastro-oesophageal measurements. Sens. Actuators B Chem. **29**, 164–168 (1995)
8. F. Baldini, S. Bracci, F. Cosi, P. Bechi, F. Pucciani, Controlled-pore glasses embedded in plastic optical fibers for gastric pH sensing purposes. Appl. Spectrosc. **48**, 549–552 (1994)
9. F. Baldini, L. Ciaccheri, A. Falai, A.G. Mignani, J. Rayss, G. Sudolski, Thymol blue immobilized on tapered fibres as an optical transducer for pH sensing. Chem. Biochem. Environ. Fiber Sens. X **3540**, 28–33 (1999)
10. M. Becker, M. Rothhardt, K. Schröder, S. Voigt, J. Mehner, A. Teubner, T. Lüpke, C. Thieroff, M. Krüger, C. Chojetzki, Characterization of fiber Bragg grating-based sensor array for high resolution manometry. Proc. SPIE **8439** (2012)
11. E. Benito-Pane, M. Granda Valdes, B. Glahn-Martinez, M.C. Moreno Bondi, Fluorescence based fiber optic and planar waveguide biosensors. A review. Anal. Chim. Acta **943**, 17–40 (2016)
12. R.P. Betts, T. Duckworth, I.G. Austin, S.P. Crocker, S. Moore, Critical light reflection at a plastic/glass interface and its application to foot pressure measurements. J. Med. Eng. Technol. **4**(3), 136–142 (1980)
13. T.A. Birks, Y.W. Li, The shape of fiber tapers. J. Lightwave Technol. **10**, 432–438 (1992)
14. D.R. Biswas, Optical fiber coatings for biomedical applications. Opt. Eng. **31**(7), 1400 (1992)
15. S.M. Borisov, O.S. Wolfbeis, Optical biosensors. Chem. Rev. **108**(2), 423–461 (2008)
16. G. Brambilla, Optical fibre nanowires and microwires: a review. J. Opt. **12**, 043001 (2010)
17. G. Brambilla, E. Koizumi, X. Feng, D.J. Richardson, Compound-glass optical nanowires. Electron. Lett. **41**, 400–402 (2005)
18. M. Brenci, G. Conforti, R. Falciai, A.G. Mignani, A.M. Scheggi, All-fibre temperature sensor. Int. J. Opt. Sens. **1** (1986)
19. I.L. Bundalo, R. Lwin, L. Leon-Saval, A. Argyros, All-plastic fiber-based pressure sensor. Appl. Opt. **55**(4), 811–816 (2016)
20. Y. Chen, Y. Ming, W. Guo, F. Xu, Y.-Q. Lu, Temperature characteristics of microfiber coil resonators embedded in Teflon, in *Passive Components and Fiber-Based Devices VIII, Proceedings of SPIE-OSA-IEEE Asia Communications and Photonics* (2012), p. 830711-1-4
21. Y. Chen, F. Xu, Y.Q. Lu, Teflon-coated microfiber resonator with weak temperature dependence. Opt. Express **19**, 22923–22928 (2011)
22. E. Cibula, D. Donlagic, Miniature fiber-optic pressure sensor with a polymer diaphragm. Appl. Opt. **44**(14), 2736–2744 (2005)
23. E. Cibula, S. Pevec, B. Lenardič, É. Pinet, D. Donlagic, Miniature all-glass robust pressure sensor. Opt. Express **17**(7), 5098–5106 (2009)
24. T. Cižmár, K. Dholakia, Exploiting multimode waveguides for pure fibre-based imaging. Nat. Commun. **3**, 1027 (2012)
25. P.S. Cottler, W.R. Karpen, D.A. Morrow, K.R. Kaufman, Performance characteristics of a new generation pressure microsensor for physiologic applications. Ann. Biomed. Eng. **37**(8), 1638–1645 (2009)
26. A.G. Crenshaw, J.R. Styf, S.J. Mubarak, A.R. Hargens, A new "transducer-tipped" fiber optic catheter for measuring intramuscular pressures. J. Orthop. Res. **8**(3), 464–468 (1990)
27. B.M. Cullum, G.D. Griffin, G.H. Miller, T. Vo-Dinh, Intracellular measurements in mammary carcinoma cells using fiber-optic nanosensors. Anal. Biochem. **277**, 25–32 (2000)
28. C.M. Davis, E.F. Carome, M.H. Weik, S. Ezekiel, R.E. Einzig, *Fiber Optic Sensor Technology Handbook* (Dynamic Systems, Reston, Virginia, 1982)
29. R.A. De Blasi, G. Conti, M. Antonelli, M. Bufi, A. Gasparetto, A fibre optics system for the evaluation of airway pressure in mechanically ventilated patients. Intensive Care Med. **18**(7), 405–409 (1992)

30. F.F.M. de Mul, L. Scalise, A.L. Petoukhova, M. van Herwijnen, P. Moes, W. Steenbergen, Glass-fiber self-mixing intra-arterial laser Doppler velocimetry: signal stability and feedback analysis. Appl. Opt. **41**(4), 658–667 (2002)
31. M. Ding, P.F. Wang, G. Brambilla, A microfiber coupler tip thermometer. Opt. Express **20**, 5402–5408 (2012)
32. P.G. Dinning, L. Wiklendt, I. Gibbins, V. Patton, P. Bampton, D.Z. Lubowski, I.J. Cook, J.W. Arkwright, Low-resolution colonic manometry leads to a gross misinterpretation of the frequency and polarity of propagating sequences: Initial results from fiber-optic high-resolution manometry studies. Neurogastroenterol. Motil. **25**, 640–649 (2013)
33. A.W. Domanski, T.R. Wolinski, W. Borys, Fiber-optic liquid crystalline high-sensitivity temperature sensor. SPIE Proc. Fiber Opt. Laser Sensor VIII **1169**, 573–581 (1990)
34. D. Donlagic, E. Cibula, All-fiber high-sensitivity pressure sensor with SiO_2 diaphragm. Opt. Lett. **30**(16), 2071–2073 (2005)
35. J.M. Edmonson, History of the instruments for gastrointestinal endoscopy. Gastrointest. Endosc. **37**, S27–S56 (1991)
36. G. Emiliyanov, P.E. Hoiby, L.H. Pedersen, O. Bang, Selective serial multi-antibody biosensing with TOPAS microstructured polymer optical fibers. Sensors **13**(3), 3242–3251 (2013)
37. T. Erdogan, Fiber grating spectra. J. Lightwave Technol. **15**(8), 1277–1294 (1997)
38. J. Feng, M. Ding, J.L. Kou, F. Xu, Y.Q. Lu, An optical fiber tip micrograting thermometer. IEEE Photonics J. **3**, 810–814 (2011)
39. J.A. Ferguson, T.C. Boles, C.P. Adams, D.R. Walt, A fiber-optic DNA biosensor microarray for the analysis of gene expression. Nat. Biotechnol. **14**, 1681–1684 (1996)
40. K.H. Frank, M. Kessler, K. Appelbaum, W. Dummler, The Erlangen micro-lightguide spectrophotometer EMPHO-I. Phys. Med. Biol. **34**, 1883–1900 (1989)
41. S.M. Gautier, L.J. Blum, P.R. Coulet, Multi-function fibre-optic sensor for bioluminescent flow determination of ATP or NADH. Anal. Chim. Acta **235**, 243–253 (1990)
42. J.L. Gehrich, D.W. Lubbers, N. Opitz, D.R. Hansmann, W.W. Miller, J.K. Tusa, M. Yafuso, Optical fluorescence and its application to an intravascular blood-gas monitoring-system. IEEE Trans. Biomed. Eng. **33**, 117–132 (1986)
43. T.G. Giallorenzi, J.A. Bucaro, A. Dandridge, G.H. Sigel, J.H. Cole, S.C. Rashleigh, R.G. Priest, Optical fiber sensor technology. IEEE J. Quantum Electron. **18**, 626–665 (1982)
44. D. Gloge, Weakly guiding fibers. Appl. Opt. **10**, 2252–2258 (1971)
45. K.T.V. Grattan, B.T. Meggitt, *Optical Fiber Sensor Technology: Fundamentals* (Kluwer Academic Publishers, Nertherlands, 2000)
46. K.T.V. Grattan, T. Sun, Fiber optic sensor technology: an overview. Sens. Actuators Phys. **82**, 40–61 (2000)
47. F.X. Gu, L. Zhang, X.F. Yin, L.M. Tong, Polymer single-nanowire optical sensors. Nano Lett. **8**, 2757–2761 (2008)
48. R.Y. Gu, R.N. Mahalati, J.M. Kahn, Design of flexible multi-mode fiber endoscope. Opt. Express **23**(21), 26905–26918 (2015)
49. M.L. Guo, J.C. Shi, B.J. Li, Polymer-based micro/nanowire structures for three-dimensional photonic integrations. Opt. Lett. **33**, 2104–2106 (2008)
50. T. Hansen, A fiberoptic micro-tip pressure transducer for medical applications. Sens. Actuators **4**, 545–554 (1983)
51. T. Hansen, A. Munkhaugen, Fiber-optic sensors for medical and electrotechnical applications using bifurcated fiber bundles. IEEE J. Quantum Electron. **17**, 2530 (1981)
52. J.Z. Hao, K.M. Tan, S.C. Tjin, C.Y. Liaw, P.R. Chaudhuri, X. Guo, C. Lu, Design of a foot-pressure monitoring transducer for diabetic patients based on FBG sensors, in *The 16th Annual Meeting of the IEEE Lasers and Electro-Optics Society, 2003. LEOS 2003* (2003)
53. K. Harada, M. Tamura, M. Toyono, Noninvasive visualization and measurement of middle cardiac vein flow by transthoracic Doppler echocardiography. Pediatr. Cardiol. **27**(6), 679–684 (2006)
54. S.A. Harfenist, S.D. Cambron, E.W. Nelson, S.M. Berry, A.W. Isham, M.M. Crain, K.M. Walsh, R.S. Keynton, R.W. Cohn, Direct drawing of suspended filamentary micro- and nanostructures from liquid polymers. Nano Lett. **4**, 1931–1937 (2004)

55. S.W. Harun, A.A. Jasim, H.A. Rahman, M.Z. Muhammad, H. Ahmad, Micro-ball lensed fiber-based glucose sensor. IEEE Photonics J. **13**, 348–350 (2013)
56. S. Haxha, A. Teyeb, F.A. Malek, E.K. Akowuah, I. Dayoub, Design of environmental biosensor based on photonic crystal fiber with bends using finite element method. Opt. Photonics J. **5**(3), 69–78 (2015)
57. B.G. Healey, L. Li, D.R. Walt, Multianalyte biosensors on optical imaging bundles. Biosens. Bioelectron. **12**, 521–529 (1997)
58. P. Hilton, C.J. Mayne, Urethral pressure measurement: a comparison of profiles obtained by conventional and fibre-optic microtransducers. Neurol. Urodyn. **8**(5), 481–489 (1989)
59. T. Hirschfeld, F. Miller, S. Thomas, H. Miller, F. Milanovich, R.W. Gaver, Laser-fiber-optic optrode for real-time invivo blood carbon-dioxide level monitoring. J. Lightwave Technol. **5**, 1027–1033 (1987)
60. T. Hirshfeld, Total reflection fluorescence. Can. J. Spectrosc. **10**, 128 (1965)
61. G.A. Holst, T. Koster, E. Voges, D.W. Lubbers, Flox—an oxygen-flux-measuring system using a phase-modulation method to evaluate the oxygen-dependent fluorescence lifetime. Sens. Actuators B Chem. **29**, 231–239 (1995)
62. H.H. Hopkins, N.S. Kapany, A flexible fiberscope using static scanning. Nature **173**, 39–41 (1954)
63. M. Hou, Y. Wang, S. Lui, J. Guo, Z. Li, P. Lu, Sensitivity-enhanced pressure sensor with hollow-core photonic crystal fiber. J. Lightwave Technol. **32**(23), 4035–4039 (2014)
64. J.B. Jensen, P.E. Hoiby, G. Emiliyanov, O. Bang, L.H. Pedersen, A. Bjarklev, Selective detection of antibodies in microstructured polymer optical fibers. Opt. Express **13**(15), 5883–5889 (2005)
65. C.K. Ji, C.L. Zhao, J. Kang, X.Y. Dong, S.Z. Jin, Multiplex and simultaneous measurement of displacement and temperature using tapered fiber and fiber Bragg grating. Rev. Sci. Instrum. **83**, 053109 (2012)
66. J. Jung, H. Nam, J.H. Lee, N. Park, B. Lee, Simultaneous measurement of strain and temperature by use of a single-fiber Bragg grating and an erbium-doped fiber amplifier. Appl. Opt. **38**, 2749–2751 (1999)
67. F. Kajiya, O. Hiramatsu, K. Mito, Y. Ogasawara, K. Tsujioka, A study of coronary circulation by laser doppler velocimetry. Med. Prog. Technol. **12**, 77–85 (1987)
68. F. Kajiya, O. Hiramatsu, K. Mito, Y. Ogasawara, K. Mito, K. Tsujioka, An optical-fiber laser doppler-velocimeter and its application to measurements of coronary blood-flow velocities, in *Regulation of Coronary Blood Flow* (Springer Japan KK, 1991), pp. 11–23
69. N.S. Kapany, N. Silbertrust, Fiber optics spectrophotometer for in-vivo oximetry. Nature **204**, 138–142 (1964)
70. P.M. Kasili, J.M. Song, T. Vo-Dinh, Optical sensor for the detection of caspase-9 activity in a single cell. J. Am. Chem. Soc. **126**, 2799–2806 (2004)
71. R.M. Kasili, B.M. Cullum, G.D. Griffin, T. Vo-Dinh, Nanosensor for in vivo measurement of the carcinogen benzo[a]pyrene in a single cell. J. Nanosci. Nanotechnol. **2**, 653–658 (2002)
72. D. Kilpatrick, F. Kajiya, Y. Ogasawara, Fibre optic laser Doppler measurement of intravascular velocity. Australas. Phys. Eng. Sci. Med. **11**, 5–14 (1988)
73. Y. Kim, S. Warren, J. Knight, M. Neil, C. Paterson, J. Stone, C. Dunsby, P. French, Adaptive multiphoton endomicroscope incorporating a polarization-maintaining multicore optical fiber. IEEE J. Sel. Top. Quantum Electron. **22**(3), 6800708 (2016)
74. Y. Kim, S. Warren, F. Favero, J. Stone, J. Clegg, M. Neil, C. Paterson, J. Knight, P. French, C. Dunsby, Semi-random multicore fibre design for adaptive multiphoton endoscopy. Opt. Lett. **26**(3), 3661–3673 (2018)
75. R. Kist, S. Drope, H. Wolfelschneider, Fiber-Fabry-Perot (FFP) thermometer for medical applications. Proc. Soc. Photo Opt. Instrum. Eng. **514**, 165–170 (1984)
76. K. Kobayashi, H. Okuyama, T. Kato, T. Yasuda, Fiberoptic catheter-tip micromanometer. Iyodenshi To Seitai Kogaku **15**(7), 465–472 (1977)
77. J.L. Kou, J. Feng, L. Ye, F. Xu, Y.Q. Lu, Miniaturized fiber taper reflective interferometer for high temperature measurement. Opt. Express **18**, 14245–14250 (2010)

78. J.L. Kou, S.J. Qiu, F. Xu, Y.Q. Lu, Demonstration of a compact temperature sensor based on first-order Bragg grating in a tapered fiber probe. Opt. Express **19**, 18452–18457 (2011)
79. V.I. Krasovskii, I.N. Feofanov, P.I. Ivashkin, M.A. Kazaryan, A fiber-optic Doppler blood flow-velocity sensor. St. Petersburg Polytech. Univ. J. Phys. Math. **3**(1), 35–38 (2017)
80. M.N. Kronick, W.A. Little, A new immunoassay based on fluorescence excitation by internal reflection spectroscopy. J. Immunol. Methods **1975**, 235–240 (1975)
81. C.M. Lawson, V.J. Tekippe, Fiber-optic diaphragm-curvature pressure transducer. Opt. Lett. **8**, 286–288 (1983)
82. A. Lekholm, L.H. Lindström, Optoelectronic transducer for intravascular measurements of pressure variations. Med. Biol. Eng. Comput. **7**(3), 333–335 (1969)
83. S.G. Leon-Saval, T.A. Birks, J. Bland-Hawthorn, M. Englund, Multimode fiber devices with single-mode performance. Opt. Lett. **30**(19), 2545–2547 (2005)
84. S.G. Leon-Saval, N.K. Fontaine, R. Amezcua-Correa, Photonic lantern as mode multiplexer for multimode optical communications. Opt. Fiber Technol. **35**, 46–55 (2017)
85. A. Leung, P. Mohana Shankar, R. Mutharasan, A review of fiber-optics biosensors. Sens. Actuators B: Chem. **125**(2), 688–703 (2007)
86. Q. Li, S.S. Wang, Y.T. Chen, M. Yan, L.M. Tong, M. Qiu, Experimental demonstration of plasmon propagation, coupling, and splitting in silver nanowire at 1550-nm wavelength. IEEE J. Sel. Top. Quantum Electron. **17**, 1107–1111 (2011)
87. L.H. Lindström, Miniaturized pressure transducer intended for intravascular use. IEEE Trans. Bio-Med. Eng. **BME-17**(3), 207–219 (1970)
88. X.J. Liu, W. Farmerie, S. Schuster, W.H. Tan, Molecular beacons for DNA biosensors with micrometer to submicrometer dimensions. Anal. Biochem. **283**, 56–63 (2000)
89. P. Lu, J. Harris, Y. Xu, Y. Lu, L. Chen, X. Bao, Simultaneous refractive index and temperature measurements using a tapered bend-resistant fiber interferometer. Opt. Lett. **37**, 4567–4569 (2012)
90. P. Lu, L.Q. Men, K. Sooley, Q.Y. Chen, Tapered fiber Mach-Zehnder interferometer for simultaneous measurement of refractive index and temperature. Appl. Phys. Lett. **94**, 131110 (2009)
91. D.W. Lubbers, Chemical in vivo monitoring by optical sensors in medicine. Sens. Actuators B Chem. **11**, 253–262 (1993)
92. E.C. Magi, L.B. Fu, H.C. Nguyen, M.R.E. Lamont, D.I. Yeom, B.J. Eggleton, Enhanced Kerr nonlinearity in sub-wavelength diameter As_2Se_3 chalcogenide fiber tapers. Opt. Express **15**, 10324–10329 (2007)
93. R.N. Mahalati, R.Y. Gu, J.M. Kahn, Resolution limits for imaging through multi-mode fiber. Opt. Express **21**(2), 1656–1668 (2013)
94. M. Makiniemi, H. Kopola, K. Oikarinen, E. Herrala, A novel fibre optic dental pulp vitalometer, in *Proceedings of Medical Sensors II and Fiber Optic Sensors*, vol. 2331 (1995), pp. 140–148
95. H. Matsumoto, M. Saegusa, K. Saito, K. Mizoi, Development of a fiber optic catheter tip pressure transducer. J. Med. Eng. Technol. **2**, 239–242 (1978)
96. M.J. Milano, K.Y. Kim, Diode array spectrometer for the simultaneous determination of hemoglobin in whole blood. Anal. Chem. **49**, 555–561 (1977)
97. A. Mills, A. Lepre, L. Wild, Breath-by-breath measurement of carbon dioxide using a plastic film optical sensor. Sens. Actuators B Chem. **39**, 419–425 (1997)
98. K. Mito, Y. Ogasawara, O. Hiramatsu, K. Tsujioka, F. Kajiya, A laser Doppler catheter for monitoring both phase and mean coronary vein flow. Heart Vessels **6**(1), 1–8 (1990)
99. K. Mito, Y. Ogasawara, O. Hiramatsu, Y. Wada, K. Tsujioka, F. Kajiya, Evaluation of blood flow velocity waveforms in intramyocardial artery and vein by laser Doppler velocimeter with an optical fiber, in *Microcirculation in Circulatory Disorders*, ed. by H. Manabe, B.W. Zweifach, K. Messmer (Springer, Tokyo, 1988), pp. 525–528
100. S. Morikawa, Fiberoptic catheter-tip pressure transducer. Iyodenshi To Seitai Kogaku **10**(1), 36–39 (1972)

101. M. Nakhostine, J.R. Styf, S. van Leufen, A.R. Hargens, D.H. Gershuni, Intramuscular pressure varies with depth: the tibialis anterior muscle studied in 12 volunteers. Acta Orthop. Scand. **64**(3), 377–381 (1993)
102. A.S. Nain, J.C. Wong, C. Amon, M. Sitti, Drawing suspended polymer micro-/nanofibers using glass micropipettes. Appl. Phys. Lett. **89**, 183105–183107 (2006)
103. E.J. Netto, J.I. Peterson, M. Mcshane, V. Hampshire, A fiber-optic broad-range pH sensor system for gastric measurements. Sens. Actuators B Chem. **29**, 157–163 (1995)
104. M. Norgia, A. Pesatori, L. Rovati, Self-mixing laser Doppler: a model for extracorporeal blood flow measurement, in *2010 IEEE Instrumentation and Measurement Technology Conference (I2MTC)*, Austin, TX, pp. 304–307, 3–6 May 2010
105. M. Norgia, A. Pesatori, L. Rovati, Self-mixing laser Doppler spectra of extracorporeal blood flow: a theoretical and experimental study. IEEE Sens. J. **12**, 552–557 (2012)
106. K. Okamoto, *Fundamentals of Optical Waveguides* (Academic Press Ed., 2000)
107. R.C. Ostrup, T.G. Luerssen, L.F. Marshall, M.H. Zornow, Continuous monitoring of intracranial pressure with a miniaturized fiberoptic device. J. Neurosurg. **67**(2), 206–209 (1987)
108. C. Ovren, M. Adolfsson, B. Hok, Fiberoptic systems for temperature and vibration measurements in industrial applications. Opt. Lasers Eng. **5** (1984)
109. J.I. Peterson, R.V. Fitzgerald, D.K. Buckhold, Fiber-optic probe for in vivo measurement of oxygen partial pressure. Anal. Chem. **56**, 62–67 (1984)
110. E. Pinet, A. Pham, S. Rioux, Miniature fiber optic pressure sensor for medical applications: an opportunity for intra-aortic balloon pumping (IABP) therapy, in *Proceedings SPIE Volume 5855, 17th International Conference on Optical Fibre Sensors* (2005). https://doi.org/10.1117/12.623806
111. M. Plaschke, M. Geyer, J. Reichert, H.J. Ache, Submicron fiber-optic sensors for calcium-ions and pH with internal calibration. Chem. Biochem. Environ. Fiber Sens. IX **3105**, 31–37 (1997)
112. N. Pleros, G.T. Kanellos, G. Papaioannou, Optical fiber sensors in orthopedic biomechanics and rehabilitation, in *9th International Conference on Information Technology and Applications in Biomedicine, 2009. ITAB 2009* (2010). https://doi.org/10.1109/itab.2009.5394386
113. S. Poeggel, D. Tosi, D. Duraibabu, G. Leen, D. McGrath, E. Lewis, Optical fibre pressure sensors in medical applications. Sensors **15**, 17115–17148 (2015)
114. G. Rajan, S. Mathews, G. Farrell, Y. Semenova, A liquid crystal coated tapered photonic crystal fiber interferometer. J. Opt. **13**, 015403 (2011)
115. Y.J. Rao, B. Hurle, D.J. Webb, D.A. Jackson, L. Zhang, I. Bennion, In-situ temperature monitoring in NMR machines with a prototype in-fiber Bragg grating sensor system, in *12th Optical Fiber Sensors (OFS-12)*, Williamsburg (1997)
116. L. Rindorf, J.B. Jensen, M. Dufva, L.H. Pedersen, P.E. Høiby, O. Bang, Photonic crystal fiber long-period gratings for biochemical sensing. Opt. Express **14**, 8224–8231 (2006)
117. L. Rindorf, O. Bang, Highly sensitive refractometer with a photonic-crystal-fiber long-period grating. Opt. Lett. **33**, 563–565 (2008)
118. P. Roriz, O. Frazao, A.B. Lobo-Ribeiro, J.L. Santos, J.A. Simoes, Review of fiber-optic pressure sensors for biomedical and biomechanical applications. J. Biomed. Opt. **18**(5), 050903 (2013)
119. Z. Rosenzweig, R. Kopelman, Development of a submicrometer optical-fiber oxygen sensor. Anal. Chem. **67**, 2650–2654 (1995)
120. P. Russell, Photonic crystal fibers. Science **299**, 358–362 (2003)
121. E. Samset, T. Mala, R. Ellingsen, I. Gladhaug, O. Søreide, E. Fosse, Temperature measurement in soft tissue using a distributed fibre Bragg-grating sensor system. Minim. Invasive Ther. Allied Technol. **10**(2), 89–93 (2009)
122. C. Scoggin, L. Nett, T.L. Petty, Clinical evaluation of a new ear oximeter. Heart Lung **6**, 121–126 (1977)

123. A.B. Seddon, A prospective for new mid-infrared medical endoscopy using chalcogenide glasses. Int. J. Appl. Glass Sci. **2**(3), 177–191 (2011)
124. O.M. Sejersted, A.R. Hargens, K.R. Kardel, P. Blom, O. Jensen, L. Hermansen, Intramuscular fluid pressure during isometric contraction of human skeletal muscle. J. Appl. Physiol. **56**(2), 287–295 (1984)
125. Y. Semenova, L. Bo, S. Mathews, P. Wang, Q. Wu, G. Farrell, Spectral tuning of a microfiber coupler with a liquid crystal overlay, in *OFS 22nd International Conference on Optical Fiber Sensors* (2012), p. 842184-1-4
126. R. Singh, A.J. Ranieri Jr., H.R. Vest Jr., D.L. Bowers, J.F. Dammann Jr., Simultaneous determinations of cardiac output by thermal dilution, fiberoptic and dye-dilution methods. Am. J. Cardiol. **25**(5), 579–587 (1970)
127. A.W. Snyder, Asymptotic expression for eigenfunctions and eigenvalues of dielectric optical waveguides. IEEE Trans. Microw. Theory Tech. **MTT-17**, 1130–1138 (1969)
128. A.W. Snyder, R.M. De La Rue, Asymptotic solution of eigenvalue equations for surface waveguide structures. IEEE Trans. MTT **MTT-18**, 650–651 (1970)
129. A.W. Snyder, J.D. Love, *Optical Waveguide Theory* (Springer ed., 1983)
130. A.B. Socorro, I. Del Villar, J.M. Corres, F.J. Arregui, I.R. Matias, Tapered single-mode optical fiber pH sensor based on lossy mode resonances generated by a polymeric thin-film. IEEE Sens. J. **12**, 2598–2603 (2012)
131. S. Sondergaard, S. Karason, A. Hanson, K. Nilsson, S. Hojer, S. Lundin, O. Stenqvist, Direct measurement of intratracheal pressure in pediatric respiratory monitoring. Pediatr. Res. **51**(3), 339–345 (2002)
132. S. Sondergaard, S. Karason, S. Lundin, O. Stenqvist, Fibre-optic measurement of tracheal pressure in paediatric endotracheal tubes. Eur. J. Anaesthesiol. **18**, 24–25 (2001)
133. E. Stefansson, J.I. Peterson, Y.H. Wang, Intraocular oxygen-tension measured with a fiber-optic sensor in normal and diabetic dogs. Am. J. Physiol. **256**, H1127–H1133 (1989)
134. A. Stiebeiner, R. Garcia-Fernandez, A. Rauschenbeutel, Design and optimization of broadband tapered optical fibers with a nanofiber waist. Opt. Express **18**, 22677–22685 (2010)
135. A. Stiebeiner, O. Rehband, R. Garcia-Fernandez, A. Rauschenbeutel, Ultra-sensitive fluorescence spectroscopy of isolated surface-adsorbed molecules using an optical nanofiber. Opt. Express **17**, 21704–21711 (2009)
136. L. Svennningsen, J. Øystein, Application of fiberoptics to the clinical measurement of intrauterine pressure in labor journal. Acta Obstet. Gynecol. Scand. **65**(6), 551–555 (1985)
137. L. Svennningsen, J. Øystein, M.S. Dodgson, A fibreoptic pressure transducer for intrauterine monitoring, in *Fetal Physiological Measurements* (1986), pp. 15–21
138. G.A. Tait, R.B. Young, G.J. Wilson, D.J. Steward, D.C. Macgregor, Myocardial pH during regional ischemia—evaluation of a fiber-optic photometric probe. Am. J. Physiol. **243**, H027–H1031 (1982)
139. S. Takeuchi, H. Tohara, H. Kudo, K. Otsuka, H. Saito, H. Uematsu, K. Mitsubayashi, An optic pharyngeal manometric sensor for deglutition analysis. Biomed. Microdevice **9**(6), 893–899 (2007)
140. M. Takiguchi, Y. Yoshikawa, T. Yamamoto, K. Nakayama, T. Kuga, Saturated absorption spectroscopy of acetylene molecules with an optical nanofiber. Opt. Lett. **36**, 1254–1256 (2011)
141. W.H. Tan, Z.Y. Shi, S. Smith, D. Birnbaum, R. Kopelman, Submicrometer intracellular chemical optical fiber sensors. Science **258**, 778–781 (1992)
142. J.B. Taylor, B. Lown, M. Polanyi, In vivo monitoring with a fiber optic catheter. J. Am. Med. Assoc. **221**(7), 667–673 (1972)
143. K.F. Tham, S. Arulkumaran, S. Chua, C. Anandakumar, P. Singh, S.S. Ratnam, A comparison between fibreoptic and catheter-tip bridge strain gauge transducers for measurement of intrauterine pressure in labour. J. Obstet. Gynaecol. **17**(1), 83–87 (1991)
144. Y. Tian, W.H. Wang, N. Wu, X.T. Zou, X.W. Wang, Tapered optical fiber sensor for label-free detection of biomolecules. Sensors **11**, 3780–3790 (2011)

145. A.K. Tomer, A. Singh, A. Gupta, Lasers in endoscopic surgery. Int. J. Prev. Clin. Dent. Res. **3**(1), 55–57 (2015)
146. L.M. Tong, L.L. Hu, J.J. Zhang, J.R. Qiu, Q. Yang, J.Y. Lou, Y.H. Shen, J.L. He, Z.Z. Ye, Photonic nanowires directly drawn from bulk glasses. Opt. Express **14**, 82–87 (2006)
147. B.J. Tromberg, M.J. Sepaniak, T. Vo-Dinh, G.D. Griffin, Fiber-optic chemical sensors for competitive binding fluoroimmunoassay. Anal. Chem. **59**, 1226–1230 (1987)
148. C. Veilleux, R.J. Black, J. Lapierre, L.W. Reeves, Nematic liquid-crystal clad tapered optical fiber with temperature sensing properties. J. Appl. Phys. **67**, 6648–6653 (1990)
149. G. Vishnoi, T.C. Goel, P.K.C. Pillai, Spectrophotometric studies of chemical species using tapered core multimode optical fiber. Sens. Actuators B Chem. **45**, 43–48 (1997)
150. T. Vo-Dinh, Nanobiosensors: probing the sanctuary of individual living cells. J. Cell. Biochem. 154–161 (2002)
151. S. Voigt, M. Rothhardt, M. Becker, T. Lupke, C. Thieroff, A. Teubner, J. Mehner, Homogeneous catheter for esophagus high-resolution manometry using fiber Bragg gratings. Proc. SPIE **7559**, 75590B (2010)
152. G.G. Wang, P.P. Shum, H.P. Ho, X. Yu, D.J.J. Hu, Y. Cui, L.M. Tong, C.L. Lin, Modeling and analysis of localized biosensing and index sensing by introducing effective phase shift in microfiber Bragg grating (mu FBG). Opt. Express **19**, 8930–8938 (2011)
153. F. Warken, E. Vetsch, D. Meschede, M. Sokolowski, A. Rauschenbeutel, Ultra-sensitive surface absorption spectroscopy using sub-wavelength diameter optical fibers. Opt. Express **15**, 11952–11958 (2007)
154. S.C. Warren, Y. Kim, J.M. Stone, C. Mitchell, J.C. Knight, M.A.A. Neil, C. Paterson, P.M.W. French, C. Dunsby, Adaptive multiphoton endomicroscopy through a dynamically deformed multicore optical fiber using proximal detection. Opt. Express **24**(19), 21474–21484 (2016)
155. R.M. Watson, D.R. Markle, Y.M. Ro, S.R. Goldstein, D.A. Mcguire, J.I. Peterson, R.E. Patterson, Transmural pH gradient in canine myocardial ischemia. Am. J. Physiol. **246**, H232–H238 (1984)
156. K.A. Wickersheim, M.H. Sun, Fiberoptic thermometry and its applications. J. Microw. Power Electromagn. Energy **22**, 85–94 (1987)
157. P.J. Wiejata, P.M. Shankar, R. Mutharasan, Fluorescent sensing using biconical tapers. Sens. Actuators B Chem. **96**, 315–320 (2003)
158. H.A.C. Wood, K. Harrington, T.A. Birks, J.C. Knight, J.M. Stone, High-resolution air-clad imaging fibers. Opt. Lett. **43**(21), 5311–5314 (2018)
159. X.B. Xing, Y.Q. Wang, B.J. Li, Nanofiber drawing and nanodevice assembly in poly(trimethylene terephthalate). Opt. Express **16**, 10815–10822 (2008)
160. B. Yang, W. Zhang, J. Zhou, H. Gui, L. Lu, B. Yu, Influence of external objects scattering property on self-mixing signal inside fiber laser. Opt. Int. J. Light Electron Opt. **125**(9), 2160–2163 (2014)
161. Y. Yang, Z. Ding, J. Meng, L. Wu, Z. He, T. Wu, M. Chen, Common path endoscopic optical coherence tomography with outside path length compensation. Proc. SPIE **6826**, 68261S (2007)
162. F.J. Zhang, B. Wang, F.F. Pang, T.Y. Wang, A luminescent temperature sensor based on a tapered optical fiber coated with quantum dots. Opt. Sens. Biophotonics II **7990**, 312–313 (2011)
163. L. Zhang, P. Wang, Y. Xiao, H.K. Yu, L.M. Tong, Ultra-sensitive microfibre absorption detection in a microfluidic chip. Lab Chip **11**, 3720–3724 (2011)
164. X. Zhang, J. Li, Y. Li, W. Wang, F. Pang, Y. Liu, T. Wang, Sensing properties of intrinsic Fabry-Perot interferometers in fiber tapers, in *OFS 22nd International Conference on Optical Fiber Sensors* (2012), p. 842189-1-4
165. X.T. Zheng, C.M. Li, Single living cell detection of telomerase over-expression for cancer detection by an optical fiber nanobiosensor. Biosens. Bioelectron. **25**, 1548–1552 (2010)
166. S. Zhu, F.F. Pang, T.Y. Wang, Single-mode tapered optical fiber for temperature sensor based on multimode interference. Opt. Sens. Biophotonics III **8311**, 83112B (2011)